buildings

MDPI

Article

Multi-Scale Optimization of Volcanic Scoria Lightweight Aggregate Concrete via Synergistic Incorporation of Styrene-Acrylic Emulsion, Foaming Agent, and Straw Fibers

Jinhong Zhang [1,2,3], Rong Li [4] and Guihua Xu [1,*]

[1] School of Light Industry Science and Engineering, Beijing Technology and Business University, Beijing 100048, China; monkey00kobe@163.com
[2] School of Materials Science and Engineering, Jilin Jianzhu University, Changchun 130000, China
[3] Jiangsu Qiqing New Material Technology Co., Ltd., Qidong, Nantong 226000, China
[4] School of Intelligent Construction, Wuxi Taihu University, Wuxi 214000, China; 18655150615@163.com
* Correspondence: ghxu@btbu.edu.cn

Abstract

Volcanic Scoria Lightweight Aggregate Concrete (VSLAC) has been identified as a material with considerable potential for use in carbon-neutral construction; however, its application is often hindered by two main issues. Firstly, the low density of scoria often results in aggregate segregation and stratification. Secondly, its high hygroscopicity can lead to shrinkage cracking. In order to address the aforementioned issues, this study proposes a multi-scale modification strategy. The cementitious matrix was first strengthened using a binary blend of Fly Ash and Ground Granulated Blast Furnace Slag (GGBS), followed by the incorporation of a ternary admixture system containing Styrene-Acrylic Emulsion (SAE), a foaming agent (FA), and alkali-treated Straw Fibres (SF) to enhance workability and durability. The findings of this study demonstrate that a mineral admixture comprising 10% Fly Ash and 10% GGBS results in a substantial enhancement of matrix compactness, culminating in a 20% increase in compressive strength. An orthogonal test was conducted to identify the optimal formulation (D13), which was found to contain 4% SAE, 0.1% FA, and 5% SF. This formulation yielded a compressive strength of 35.2 MPa, a flexural strength of 7.5 MPa, and reduced water absorption to 8.0%. A comparative analysis was conducted between the mineral admixture mix ratio (Control group) and the Optimal mix ratio (Optimization group). The results of this analysis reveal that the Optimization group exhibited superior durability and thermal characteristics. Specifically, the water penetration depth of the optimized composite was successfully restricted to within 3.18 mm, while its thermal insulation performance demonstrated a significant enhancement of 12.3%. In the context of freeze–thaw cycles, the modified concrete demonstrated notable durability, exhibiting a 51.4% reduction in strength loss and a marginal 0.64% restriction in mass loss. SEM analysis revealed that the interaction between SAE and the FA resulted in the densification of the Interfacial Transition Zone (ITZ). In addition, the 3D network formed by SF redistributed internal stresses, thereby shifting the failure mode from brittle fracture to ductile deformation. The findings demonstrate that modifying VSLAC at both micro- and macro-levels can effectively balance structural integrity with thermal efficiency for sustainable construction applications.

Keywords: Volcanic Scoria Lightweight Aggregate Concrete; synergistic modification; fly ash; Ground Granulated Blast Furnace Slag; styrene-acrylic emulsion; straw fibre; foaming agent

Check for updates

Academic Editor: César Porras-Amores

Received: 4 January 2026
Revised: 21 January 2026
Accepted: 23 January 2026
Published: 25 January 2026

Copyright: © 2026 by the authors. Licensee MDPI, Basel, Switzerland. This article is an open access article distributed under the terms and conditions of the Creative Commons Attribution (CC BY) license.

1. Introduction

Volcanic scoria is a porous lightweight aggregate formed during explosive eruptions [1]. Its incorporation into concrete has been shown to significantly reduce bulk density, typically to a range of 300–1850 kg/m^3, compared to 2200–2600 kg/m^3 for conventional concrete [2]. This lower density offers clear economic benefits by reducing structural dead loads and lowering transportation and construction costs [3]. In addition to weight reduction, scoria-based lightweight aggregate concrete (LWAC) provides enhanced thermal insulation. The cellular structure of scoria has been shown to impede heat transfer and reduce thermal conductivity, thereby enhancing building energy efficiency and curtailing operational energy consumption [4].

The ITZ is widely recognised as the critical weak link in concrete, primarily due to the inherent brittleness and high risk of autogenous shrinkage in pure Ordinary Portland cement (OPC) pastes. In order to address these limitations, the matrix is commonly modified using supplementary cementitious materials (SCMs), such as fly ash, GGBS, silica fume and rice husk ash [5,6]. In the domain of mix design, the water-to-binder (w/b) ratio exerts a significant degree of control over the process. Given the considerable variation in specific surface area and particle size distribution exhibited by many SCMs in comparison to cement clinker, the replacement of cement by mass results in a consequential alteration to the packing density of the binder. This approach has been demonstrated to refine the pore structure, thereby enhancing both matrix impermeability and volumetric stability [7–11]. Furthermore, alkali-activation of these mineral admixtures has been demonstrated to effectively regulate binder rheology, thereby improving fluidity and workability in the fresh state [12].

In order to mitigate the inherent weaknesses of LWAC—notably aggregate buoyancy and stratification caused by the density mismatch between aggregates and the matrix—various mineral admixtures, chemical additives, and fibre reinforcements have been investigated. Research has demonstrated that the pozzolanic activity of volcanic ash has a substantial effect on microstructure, thereby enhancing the binding properties of the cementitious matrix [13]. Furthermore, the synergistic effect of fibres and polymers has been demonstrated to enhance flexural performance beyond the limits of conventional reinforced concrete [14]. Geetha's report suggests that the strategic utilisation of polymers, nanomaterials, and advanced foaming techniques can circumvent conventional strength trade-offs inherent in traditional methods [15,16]. Building on this, Chen Shi demonstrated that Styrene-Butadiene Rubber latex improves interfacial bonding strength, allowing LWAC to achieve higher compressive strength and durability while maintaining its low-density profile [17,18]. Furthermore, the combination of Nano-$CaCO_3$ and superabsorbent polymers has been found to balance shrinkage mitigation and mechanical stability, effectively reducing early-age autogenous shrinkage by refining the pore structure [19]. With regard to the mechanisms of pore formation, microbial foaming agents have been demonstrated to exhibit superior stability and vesiculation. In comparison with direct mixing, the pre-foaming method results in a more uniform pore size distribution. The "Integrated Pore Influence Factor" and its associated empirical models provide a framework for quantifying the non-linear relationship between pore topology and compressive strength. Calorimetric analysis has further elucidated the compatibility between specific admixtures and protein-based foaming agents, establishing a basis for regulating the hydration kinetics of ultra-lightweight foamed concrete [20–22]. Additionally, polypropylene fibres have been demonstrated to retain their tensile capacity at elevated temperatures, thereby enabling the matrix to sustain higher stresses and effectively arresting crack propagation [23–26].

In the context of sustainable development, the valorisation of agricultural waste (natural plant fibres) and recycled aggregates as alternatives to synthetic fibres has garnered

considerable attention. As demonstrated in [27,28], the integration of corn stalk fibres with expanded polystyrene beads facilitates the production of composites that exhibit low densities and high thermal resistance. In a similar manner, the surface modification of straw fibres using nano-silica has been demonstrated to enhance the integrity of the ITZ, thus augmenting the fatigue resistance of the resultant fibre-reinforced concrete [29,30]. With regard to material substitution, the replacement of cement with wheat straw ash and silica fume in ultra-high-performance fibre-reinforced concrete has been shown to yield superior static and dynamic mechanical properties. Thermogravimetric analysis corroborated these results, confirming a denser matrix at a 90-day curing age [31]. Furthermore, the incorporation of fibres optimises the connectivity between recycled aggregates, thereby enhancing both the mechanical stability and seismic resilience of the concrete [32–34]. Utilising these insights, this study proposes an optimised VSLAC method that employs natural lightweight aggregates. The research evaluates the binary synergy of fly ash and slag in mitigating autogenous shrinkage and investigates the ternary interaction among SAE, FA, and SF through a multi-scale optimisation approach (see Figure 1). SAE targets pore stabilisation and interfacial refinement, thereby mitigating strength degradation and defects associated with the porous structure. FA facilitates density reduction and thermal isolation via void generation, thus laying the foundation for energy efficiency. SF provides a structural bridging mechanism, creating a skeletal network that enhances tensile resistance and macroscopic fracture toughness.

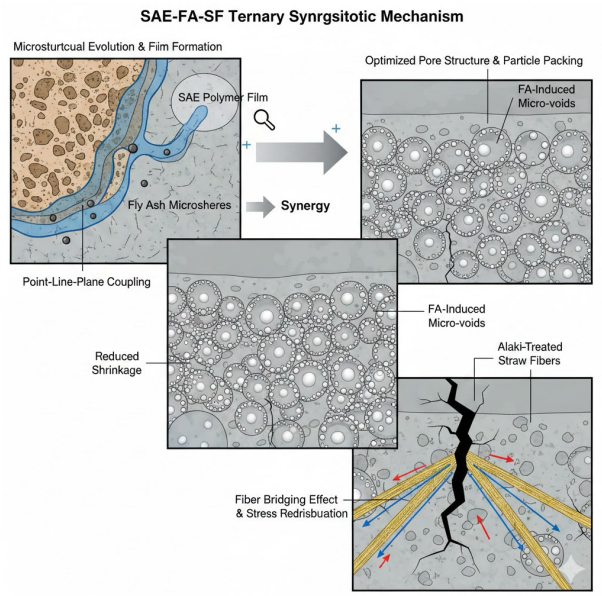


Figure 1. SAE-FA-SF ternary synergy mechanism.

The alignment of performance metrics with industrial standards is a key finding of this research, with the potential to significantly mitigate the carbon footprint of concrete production and facilitate the sustainable disposal of construction waste. These outcomes contribute to a viable strategy for resilient and sustainable infrastructure development. The comprehensive experimental methodology employed in this study is detailed in Figure 2.

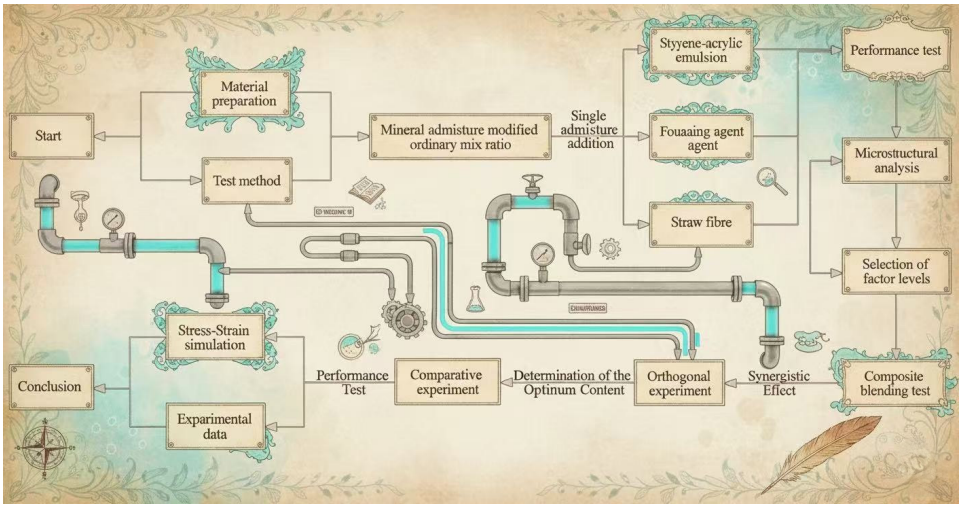


Figure 2. Experimental procedure flowchart.

2. Materials and Methods

2.1. Materials

The specific parameters and sources of the materials required for this research are shown in Table 1. The physical appearance of the volcanic ash is depicted in Figure 3a, the microscopic image is shown in Figure 3b, and the physical image of the straw fibers is presented in Figure 3c.

Table 1. Summary of raw materials and their key properties.

Material	Key Specifications/Properties	Source/Manufacturer
Volcanic Scoria (VS)	Fine: 0.15–4.75 mm; Coarse: 5–12 mm	Huinan, Jilin, China
OPC	Grade P·O 42.5; 28-day strength: 45.5 MPa	Changchun Yatai Cement Plant, ChangChun, Jilin, China
Fly Ash	Class II SCM	Compliant with national standards ChangChun, Jilin, China
GGBS	Ball-milled for 30 min	Compliant with national standards ChangChun, Jilin, China
SAE	Styrene-Acrylic Emulsion; 48.2% solid content	Guangzhou Suixin Chemical Co., Ltd. Guangzhou, Guangdong, China
FA	SDS ($C_{12}H_{25}OSO_3Na$); Krafft point of 8 °C	White powder form, ChangChun, Jilin, China
SF	Na_2SiO_3 treated [35]; Width: 0.5–2 mm; Length: 15–25 mm	Corn straw, ChangChun, Jilin, China
Superplasticizer	Polycarboxylate-based(PCE); 25% water reduction	Rheological regulator, ChangChun, Jilin, China

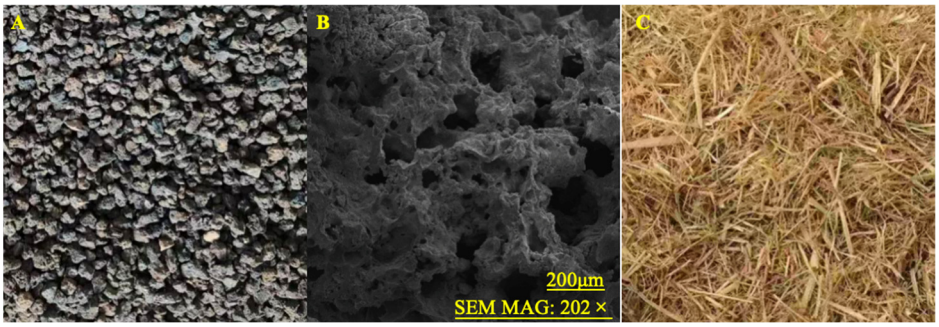


Figure 3. (**A**) Physical Image. (**B**) Microstructure of volcanic scoria. (**C**) Straw fiber.

2.2. Methods

2.2.1. Determination of Mineral Admixture Proportions

The present study investigates the synergistic potential of fly ash and GGBS as cementitious partial replacements for OPC [36]. The utilisation of these mature industrial by-products as SCMs has been demonstrated to reduce the carbon footprint and overall production costs of concrete. Furthermore, it has been shown to facilitate the valorisation of industrial waste within the framework of a circular economy.

The experimental matrix was designed to evaluate the individual and synergistic effects of fly ash and GGBS through both mono-incorporation and binary blending. These SCMs were integrated into the binder via mass replacement of cement (with proportions of 10%, 20%, and 30% of SCMs replacing cement, as detailed in Tables 2 and 3). The investigation concentrated on establishing a correlation between the mechanical properties and the microstructural evolution of the materials. Specifically, the compressive strength was measured in order to assess macro-scale performance, while the use of SEM was employed to characterise the morphological features of the matrix, with emphasis on the ITZ.

Table 2. Single admixture ratio (kg/m^3).

Group	VS	OPC	Fly Ash or GGBS	Water	PCE
a	800	450	50	275	2
b	800	400	100	275	2
c	800	350	150	275	2

Table 3. Compound admixture ratio (kg/m^3).

Group	VS	OPC	Fly Ash	GGBS	Water	PCE
1	800	400	50	50	275	2
2	800	350	50	100	275	2
3	800	300	50	150	275	2
4	800	350	100	50	275	2
5	800	300	100	100	275	2
6	800	250	100	150	275	2
7	800	300	150	50	275	2
8	800	250	150	100	275	2
9	800	200	150	150	275	2

2.2.2. Experimental Program

The present study proposes a multi-scale optimisation strategy for the purpose of enhancing the mechanical performance and durability of VSLAC through the targeted integration of chemical and mineral admixtures. In order to prevent the loss of matrix integrity associated with excessive additive concentrations, dosage levels were maintained within a 0–20% range. This constraint facilitates a rigorous quantification of both independent and synergistic effects within a tiered experimental framework.

The experimental programme commenced with the isolation of the effects of individual constituents, namely SAE (1–16%), FA (0.1–3%), and SF (1–9%), which were designated as Groups A through E (see Table 4). Preliminary results indicated the employment of an orthogonal array (Table 5) to optimise multivariate interactions for peak physicochemical performance [36]. The resulting optimal formulation was then benchmarked against a control specimen in order to verify its compliance with industrial standards and structural codes. The performance of the material was evaluated through a multi-faceted analysis, incorporating early-age (7d) and mature (28d) mechanical evolution, orthogonal experi-

ment, durability assessments, and microscopic characterisation analysis. The latter was conducted using a SEM.

Table 4. Correlation of dosage ratios.

SMs (%) Group	A	B	C	D	E
SAE	1	2	4	8	16
FA	0.1	0.5	1	2	3
SF	1	3	5	7	9
Na_2SiO_3 treated SF	1	3	5	7	9

Table 5. Orthogonal design scheme.

Experimental Group	Influencing Factors		
	SAE	FA	SF
D1	A1	B1	C1
D2	A1	B2	C2
D3	A1	B3	C3
D4	A1	B4	C4
D5	A1	B5	C5
D6	A2	B1	C5
D7	A2	B2	C1
D8	A2	B3	C2
D9	A2	B4	C3
D10	A2	B5	C4
D11	A3	B1	C4
D12	A3	B2	C5
D13	A3	B3	C1
D14	A3	B4	C2
D15	A3	B5	C3
D16	A4	B1	C3
D17	A4	B2	C4
D18	A4	B3	C5
D19	A4	B4	C1
D20	A4	B5	C2
D21	A5	B1	C2
D22	A5	B2	C3
D23	A5	B3	C4
D24	A5	B4	C5
D25	A5	B5	C1

2.2.3. Preparation Method

In order to avoid the mechanical crushing of fragile volcanic scoria and to minimise segregation caused by the density mismatch between the aggregate and the cement paste, manual mixing and consolidation were employed. The utilisation of manual protocols superseded mechanical methodologies in order to preserve the initial particle size distribution of the scoria and to impede aggregate flotation. Such measures are vital for ensuring that the measured mechanical properties accurately reflect the influence of the admixtures rather than processing-induced defects.

The preparation protocols for modified VSLAC were optimised based on the physicochemical properties of each admixture:

SAE-modified VSLAC: The styrene-acrylic emulsion was initially subjected to homogenisation with the cementitious binder. In order to maintain a constant effective

water-binder ratio, the mixing water was adjusted by subtracting the water content inherent in the emulsion [17]. The introduction of scoria aggregates was contingent upon the attainment of a uniform paste.

The present study investigates the effects of FA modification on VSLAC. The methodology involved the utilisation of a pre-foaming technique, wherein the surfactant was dissolved in water and subjected to mechanical agitation to yield a stable foam. This foam was subsequently integrated into a fresh slurry.

The SF-modified VSLAC method involved the dispersion of straw fibres within the cement paste prior to aggregate addition, with the objective of ensuring uniform distribution. In order to mitigate the inhibitory effects of residual sugars on cement hydration, an alkaline pretreatment with Na_2SiO_3 was conducted, thereby optimising interfacial bonding and hydration kinetics.

3. Results and Analysis

3.1. Influence of Mineral Admixtures on VSLAC Performance

Fly ash and GGBS, which are characterised by high reactive silica and alumina contents (SiO_2, Fe_2O_3, Al_2O_3, and CaO), act as SCMs that refine the binder matrix. It has been demonstrated that, in comparison with OPC, their higher specific surface area results in the provision of extensive nucleation sites, thereby promoting a synergistic effect through both mono and binary incorporation. This enhancement is driven by the secondary pozzolanic reaction, which consumes $Ca(OH)_2$ to form additional calcium silicate hydrate (C-S-H) gels that occupy the capillary pores. Furthermore, the "micro-filler" effect optimises particle packing, while the spherical morphology of fly ash particles induces a "ball-bearing" effect. Collectively, these mechanisms serve to reduce inter-particle friction, thereby significantly enhancing the rheological fluidity and structural density of the VSLAC.

As illustrated in Figure 4A, the experimental outcomes stemming from the exclusive incorporation of Fly Ash and GGBS, as delineated in the mix design outlined in Table 2, are presented. The data indicates that the compressive strength of VSLAC displays a parabolic evolution relative to the mineral admixture content. Peak reinforcement was observed at a 10% substitution level for both fly ash and GGBS, yielding significant strength increments of 3.6 MPa and 4.2 MPa, respectively. This enhancement in performance can be attributed to the volumetric expansion of the binder paste; the lower specific gravity of SCMs relative to OPC enhances aggregate encapsulation and interfacial bonding under a constant water-to-binder ratio. However, exceeding the 10% threshold has been shown to trigger a dilution effect and augment the specific surface area, thereby escalating water demand and compromising matrix compactness.

The binary synergy between fly ash and GGBS is further elucidated in Figure 4B, where the Group 1 configuration (10% fly ash and 10% GGBS) demonstrated a superior mechanical response, yielding a 20% strength enhancement over the control. This synergistic mechanism is rooted in the complementary nature of their physicochemical attributes. The spatial configuration of fly ash particles, which is spherical in nature, induces a phenomenon referred to as the "ball-bearing effect". This effect has been shown to optimise rheological fluidity within the system. In addition, the angular GGBS particles, due to their inherent angularity, impart a "micro-filler effect". This effect, in turn, serves to refine the particle size distribution within the cementitious system. From a kinetic perspective, the alkaline environment and nucleation sites generated during the early-stage GGBS hydration process catalyse the pozzolanic activity of the fly ash. Such multi-scale interactions effectively densify the ITZ and refine capillary porosity, thereby compensating for the inherent structural deficiencies of the scoria aggregate. The microstructural characterisation of the material was performed using a SEM, as illustrated in Figure 4C. This analysis provided

further evidence to support the macro-scale findings, revealing a highly compacted ITZ with minimal void ratios. Consequently, the Group 1 proportions were established as the benchmark for subsequent optimization phases [37–39].

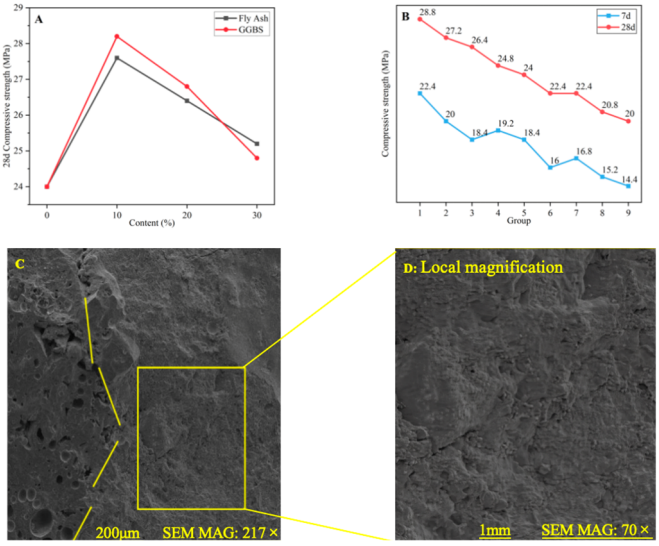


Figure 4. (**A**) Compressive strength of single mixed Fly Ash or GGBS. (**B**) Compressive strength of mixed fly ash and GGBS. (**C**) Microscopic characterization diagram of the mineral admixture mix ratio. (**D**) Local magnification.

3.2. Influence of Individual Admixtures on Performance

3.2.1. Compressive Strength

The compressive strength evolution of modified VSLAC was assessed at 7-day and 28-day curing intervals. During the initial hydration phase (a period of seven days), specimens that had undergone modification with SAE exhibited a relative retardation in strength development. This phenomenon is likely attributable to the inhibitory effect of the surfactant on cement hydration. Conversely, SF reinforcement facilitated an immediate strength gain, primarily through its effective crack-bridging mechanism during initial loading. The strength contribution of the FA remained marginal at this stage, following a more gradual progression. However, by the 28-day mark, a significant acceleration in strength gain was observed in the SAE-modified specimens. This late-stage enhancement is attributed to the formation of a continuous polymer film within the cementitious matrix, which substantially bolsters the adhesive bond strength and densifies the internal pore structure.

As illustrated in Figure 5, the compressive strength of VSLAC exhibited a non-monotonic trend relative to admixture dosage, typically reaching a maximum before a subsequent decline. In the SAE-modified series, the maximum compressive strength achieved 33.2 MPa at a 4% dosage, representing a 15.28% enhancement over the mineral admixture baseline. For the FA-modified concrete, the strength peaked at 31.4 MPa with a 0.1% dosage; however, exceeding this optimal threshold triggered a precipitous drop in performance, with a maximum reduction reaching 42%. With regard to the utilisation of fibre reinforcement, the SF-modified concrete demonstrated its optimal strength at an incorporation level of 3%, exhibiting an enhancement exceeding 10%. Moreover, longitudinal analysis has been shown to confirm that alkali-pretreated SF provides a superior reinforcing effect in comparison to untreated fibres, likely as a result of enhanced interfacial bonding [29,40–42].

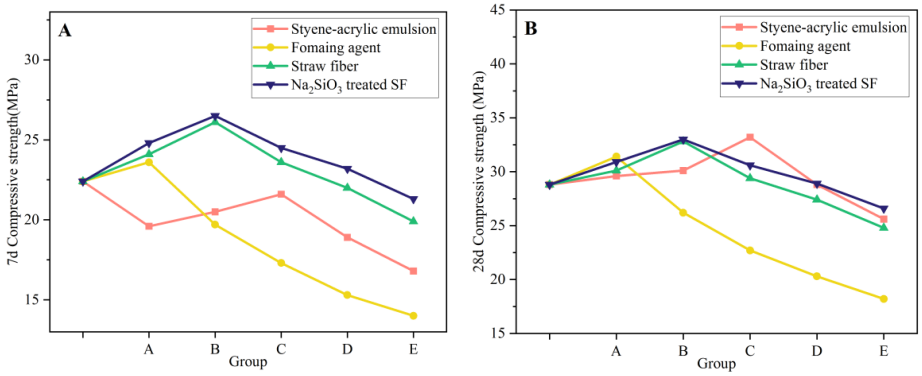


Figure 5. The effect of SAE, FA and SF on the compressive strength of VSLAC at the age of 7 days (**A**) and 28 days (**B**).

3.2.2. Flexural Strength

As illustrated in Figure 6, the flexural strength of VSLAC exhibited a parabolic evolution across all experimental groups, typically reaching a specific threshold before declining. The SAE-modified specimens exhibited a maturation profile that was consistent with their compressive behaviour: early-age strength gain remained conservative, followed by a significant acceleration as hydration reached 28 days. At an optimal concentration of 4% SAE, the flexural strength demonstrated a 40% improvement, reaching 6.8 MPa, in comparison to the control.

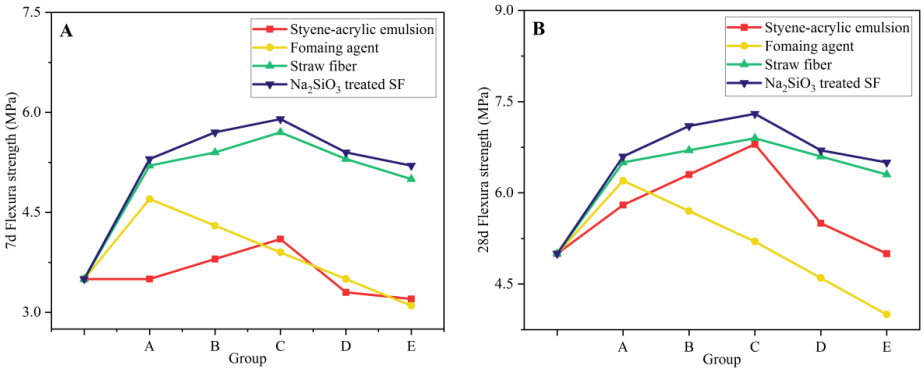


Figure 6. The effect of SAE, FA and SF on the flexural strength of VSLAC at the age of 7 days (**A**) and 28 days (**B**).

While the primary function of the FA was to optimise rheological properties, its influence on mechanical integrity was found to be dosage-dependent. A comparative analysis indicates that excessive FA incorporation introduces surplus entrained air voids, thereby triggering a degradation in structural density and mechanical performance. The FA-modified series demonstrated a maximum flexural strength of 6.2 MPa at a 0.1% dosage.

Conversely, SF utilised its inherent ductility and high tensile capacity to construct a three-dimensional bridging network within the matrix. This micro-structural framework enhances the mechanical interlocking between the binder and scoria aggregates, significantly bolstering the compactness of the composite. As demonstrated in Figure 6b, the specimens that were reinforced with SF exhibited accelerated strength development in the early stages. At a 5% SF content, the flexural strength demonstrated a peak of 7.3 MPa, which is almost 50% higher than that of the control. It is noteworthy that the 7-day strength attained 80% of the 28-day value, which is significantly higher than the conventional concrete maturation threshold of 70% [21,43]. This outcome is indicative of the immediate reinforcement provided by the fibre network.

3.2.3. Water Absorption Rate

The experimental data demonstrate that the independent incorporation of each admixture induces a non-monotonic, concave trend in water absorption (Figure 7). In the SAE-modified series, termination of capillary pathways, absorption rates across all dosages remained consistently below the control baseline. At an optimal concentration of 4% SAE, the specimens demonstrated minimum absorption values of 7.5% at 7 days and 6.8% at 28 days, representing significant reductions of 26.47% and 28.42%, respectively. With regard to the FA, the lowest absorption was achieved at a 0.1% dosage, with reductions of 10.78% (7 d) and 26.31% (28 d). However, further increases in FA content caused the absorption rate to revert toward baseline levels. This rebound is attributed to the excessive entrainment of air voids; the resulting increase in pore interconnectivity compromises both the matrix compactness and its resistance to water ingress.

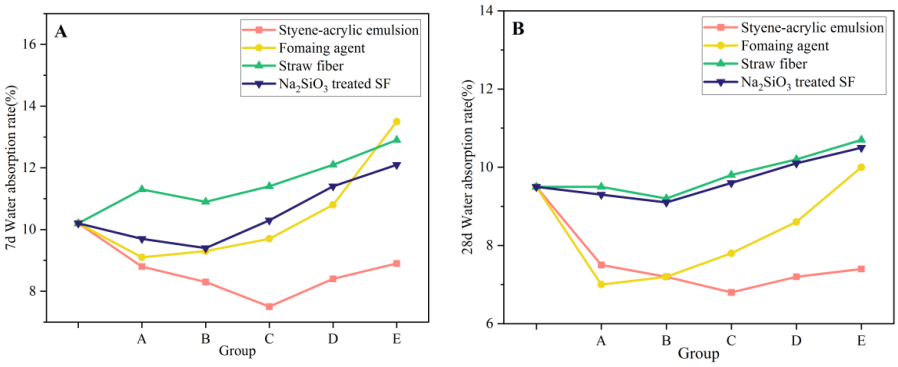


Figure 7. The effect of SAE, FA and SF on water absorption rate of VSLAC at the age of 7 days (**A**) and 28 days (**B**).

The performance of SF-modified specimens was found to be highly sensitive to surface pretreatment. Untreated SF demonstrated heightened absorption during the initial hydration phase, predominantly attributable to the intrinsic hydrophilic nature of organic polysaccharides present on the fibre surfaces. Conversely, alkali-pretreated SF (via Na_2SiO_3) demonstrated a stabilized absorption profile. This finding suggests that Na_2SiO_3 treatment is an effective method of removing organic impurities and modifying the fibre surface energy, thereby reducing its water-affinity. As demonstrated in Figure 7B, the 3% SF dosage resulted in the lowest absorption at 9.2%, which was subsequently refined to 9.1% following alkali treatment [35].

3.2.4. Thermal Conductivity and Frost Resistance

As demonstrated in Figure 8, the incorporation of SAE led to concurrent optimisation of the thermal insulation and frost resistance of the VSLAC, primarily attributable to the adhesive and film-forming properties of the polymer emulsion. It is evident that frost resistance is a pivotal metric for assessing durability. The enhanced interfacial bonding facilitated by SAE refines the internal microstructure, thereby mitigating hydraulic and osmotic pressures during the cycles of freezing and thawing. Thermal conductivity profiles indicate that at a 4% SAE dosage, the thermal conductivity was lowered to 0.1978 W/(m·K) (a 7.3% reduction). Furthermore, the compressive strength loss following freeze–thaw exposure was curtailed by nearly 30%, thereby underscoring the efficacy of the polymer-modified matrix in resisting cryogenic damage [44].

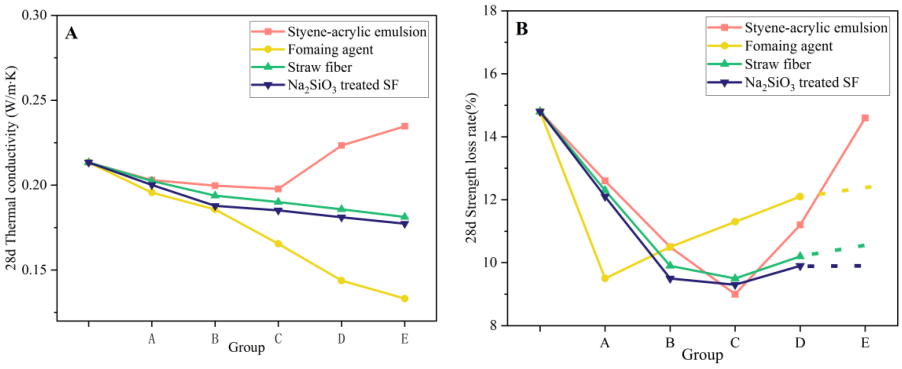


Figure 8. The effect of SAE, FA and SF on the thermal conductivity of VSLAC at the age of 28 days (**A**) and the strength loss rate of VSLAC at the age of 28 days (**B**).

It has been demonstrated by preceding studies that the effectiveness of FA and SF in increasing the thermal resistance of concrete is substantiated [14,27]. The incorporation of FA results in the formation of a dispersed gaseous phase within the cementitious matrix, thereby creating discrete, non-connected voids. These voids function to suppress heat flux via conductive pathways. Consequently, thermal conductivity exhibited a monotonic reduction relative to FA concentration. However, at elevated FA dosages (Group E), the excessive porosity triggered premature structural disintegration during freeze–thaw cycles, rendering mechanical testing unfeasible (Figure 8B). An optimised FA dosage of 0.1% resulted in a minimum compressive strength loss of 9.5%. These findings highlight a critical trade-off: while high FA concentrations favour thermal insulation, they simultaneously destabilise the matrix, compromising its resilience against frost-heave stresses. In order to achieve a synergy between thermal efficiency and frost durability, a calibrated dosage is required.

The influence of SF, a conventional insulating material in Northeast China, on thermal conductivity exhibited a downward trajectory analogous to that observed in the FA series. In relation to frost resistance, it was observed that an SF content that was above the optimal level resulted in degradation of the specimens in Group E. At a 3% SF dosage, the strength loss rates for untreated and alkali-treated fibres were 9.5% and 9.3%, respectively. The superior performance of Na_2SiO_3-pretreated SF validates the role of chemical modification in refining the fibre-matrix interface, thereby bolstering interfacial compatibility and mitigating the inherent hydrophilic defects of raw organic fibres [45,46].

3.3. Microstructural Analysis

The ITZ is conventionally identified as the most compromised phase within concrete composites under mechanical loading. In order to address this structural vulnerability, a multi-scale modification strategy was implemented, integrating the superior adhesive capacity of SAE [15], the rheological refinement of FA [20], and the inherent hygroscopicity and frictional resistance of SF [27].

During the initial hydration phase, the polymer emulsion undergoes coalescence to form a continuous film that encapsulates the binder particles. This encapsulation temporarily hinders the pozzolanic interaction between the cementitious matrix and the scoria aggregates, leading to latent development of early-age strength. As hydration progresses, the developing cementitious skeleton becomes interwoven with the polymer network, thereby enabling the initiation of secondary pozzolanic reactions at the interface. This transition has been shown to result in a substantial increase in strength gain. Experimental characterisation confirms that the polymer emulsion substantially bolsters the cohesive

forces within the ITZ, establishing robust interfacial integrity through the formation of a polymer-cement co-matrix.

The microstructure of VSLAC modified with 4% SAE is elucidated in Figure 9A. The ITZ demonstrates a high degree of compaction [17], characterised by the integration of polymer particles within the hydrated matrix. These particles offer a dual-reinforcement mechanism, occluding the capillary pores of the cement paste and penetrating the vesicular surface of the scoria aggregates. The filler effect serves to refine the pore structure, thereby enhancing both the mechanical strength and impermeability of the material.

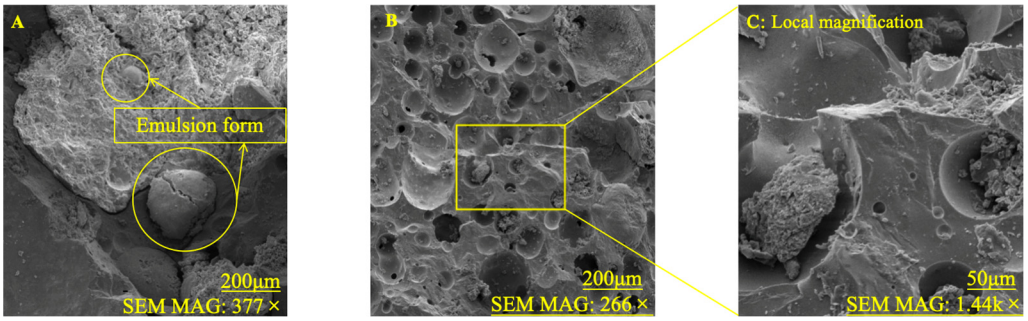


Figure 9. Microstructure of SAE modified VSLAC: (**A**) polymer emulsion in the form of VSLAC, (**B**) aggregation diagram of emulsion particles and (**C**) local magnification.

However, it was observed that there was a decline in performance at dosages that fell outside the optimal range. This degradation is attributed to the oversaturation of SAE, which hinders the uniform dispersion of the emulsion and triggers particle agglomeration (Figure 9B). In contrast to the individual particles that refine the matrix, these macro-agglomerates act as localized structural heterogeneities. It has been demonstrated that these substances impede hydration kinetics by sequestering reactive surfaces. Furthermore, they have been shown to introduce detrimental voids. Such defects function as stress concentration sites and preferential seepage pathways, ultimately undermining the mechanical integrity and long-term durability of the concrete [46–50].

The integration of a FA primarily facilitates the entrainment of stable, uniformly dispersed micro-bubbles, which serves to optimize the rheological properties and workability of fresh VSLAC. In the hardened state, this air-void system refines the particle packing configuration and reduces the system's bulk density, thereby promoting overall structural compactness. As demonstrated in Figure 10A, the calibration of the FA dosage effectively enhances the density of the ITZ, thereby reinforcing the bond between the scoria aggregates and the cementitious matrix. This microstructural refinement, in conjunction with the reduced internal porosity, directly contributes to the observed enhancements in mechanical performance. Moreover, these discrete bubbles hinder capillary suction. As hydration progresses, the maintenance of a stabilized, fine-pore network optimises the gas permeability of the composite.

However, exceeding a critical FA threshold (0.1%) has been shown to trigger an adverse morphological transition. Excessive air entrainment has been shown to induce the coalescence and coarsening of bubbles, culminating in the formation of deleterious, interconnected macropores (Figure 10B). This shift disrupts the structural continuity of the cementitious matrix, resulting in an elevation of total porosity and a compromise in interfacial adhesion. Such a degraded pore architecture precipitates a decline in mechanical strength and establishes preferential percolation pathways for moisture ingress, thereby escalating water absorption and undermining freeze–thaw durability.

The monotonic reduction in thermal conductivity relative to FA content is rooted in the evolution of the internal pore phase. The increased volume of closed pores, the low thermal

conductivity of the stagnant gaseous phase trapped within the voids, and the attenuation of convective heat transfer collectively inhibit solid-phase heat conduction. In order to achieve a synergy between mechanical integrity and long-term durability, this study identifies a low FA dosage as the optimal concentration for maintaining the microstructural stability of VSLAC [21,44–46,51].

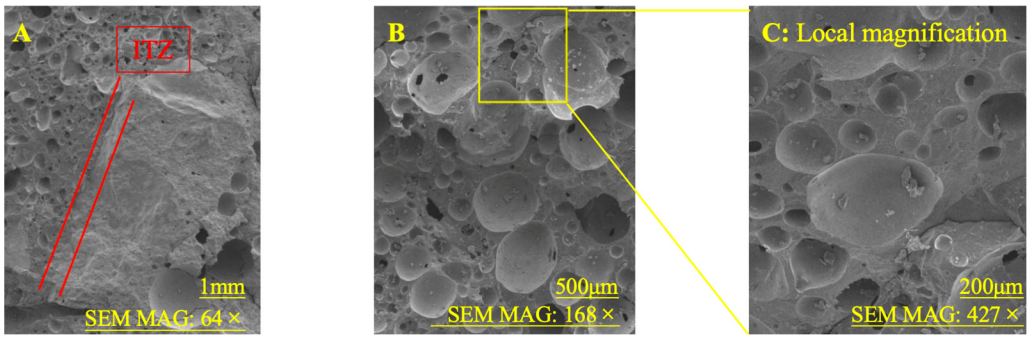


Figure 10. Microstructure of VSLAC modified with FA: (**A**) ITZ interface diagram, (**B**) internal pore structure diagram and (**C**) local magnification.

The surface of raw SF is characterised by an epicuticular waxy layer and inherent hydrophilicity. Consequently, alkaline pretreatment is necessary prior to their incorporation into the concrete matrix. The chemical modification under discussion facilitates the partial dissolution of non-cellulosic constituents, including, but not limited to, hemicellulose, lignin and pectin. The result of this process is optimised surface topography and interfacial bonding potential. As demonstrated in Figure 11A, alkali treatment has been shown to significantly elevate surface roughness, thereby yielding a more pronounced texture that enhances micro-mechanical interlocking and anchoring efficiency within the cementitious matrix. This topographical modification is instrumental in ensuring the integrity of the ITZ. However, an SF dosage that exceeds the optimal range can impede the complete encapsulation of fibres by hydration products, resulting in a compromised interface and localized porosity (Figure 11B). This, in turn, can compromise the mechanical performance of the composite.

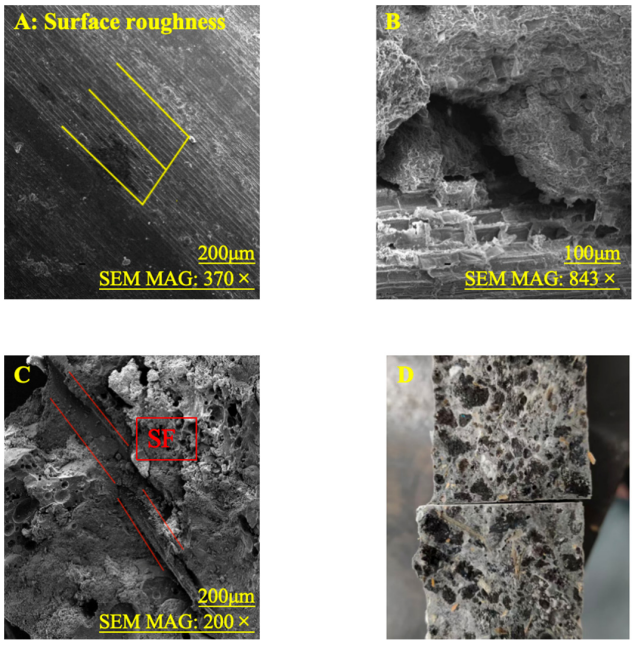


Figure 11. (**A**) Microstructure of SF. (**B**,**C**) Microstructure of VSLAC modified with FA. (**D**) Fracture surface.

The spatial distribution of SF within the matrix establishes a robust three-dimensional (3D) network (Figure 11C). In the context of mechanical loading, this skeletal architecture enables effective stress transfer and redistribution across the matrix. Consequently, the failure mechanism transitions from the brittle fracture characteristic of plain concrete to a more quasi-ductile response (Figure 11D). This shift is indicative of the crack-arresting and toughening efficacy of the SF. The synergistic mechanisms of fibre bridging and pull-out have been shown to inhibit the propagation of macro-cracks. In addition, they have been demonstrated to enhance post-peak load-bearing capacity and strain energy absorption. Furthermore, this 3D network optimises energy dissipation kinetics, thereby enhancing the seismic resilience of the VSLAC composite [27,52–55].

3.4. Results of Multi-Admixture Incorporation

3.4.1. Orthogonal Experimental Analysis

An orthogonal experimental design was implemented, utilising SAE, FA, and SF as primary factors. The levels for these variables were systematically assigned as follows: The factor SAE is measured at 1–16%, the factor FA at 0.1–3.0%, and the factor SF at 1–9%. All trials were conducted in the sequence stipulated by the $L_{25}(5^3)$ orthogonal array (see Table 5), and the comprehensive performance dataset is summarised in Table 6.

Table 6. Orthogonal test results.

Experimental Group	Compressive Strength (MPa)	Flexural Strength (MPa)	Water Absorption Rate (%)
D1	30.1	7.2	8.9
D2	28.8	7.3	9.2
D3	26.8	7.0	9.5
D4	24.4	7.0	9.6
D5	22.4	6.5	10.1
D6	23.3	6.8	9.0
D7	32.2	7.4	8.7
D8	30.1	7.3	9.5
D9	29.8	6.9	9.2
D10	27.6	6.7	10.1
D11	26.2	7.1	12.1
D12	25.3	6.9	13.4
D13	35.2	7.5	8.0
D14	30.3	6.8	8.9
D15	30.4	7.2	9.9
D16	28.8	7.1	11.8
D17	27.9	6.9	12.3
D18	25.5	6.5	14.1
D19	28.8	6.7	9.3
D20	28.9	6.8	9.5
D21	30.2	7.2	9.3
D22	29.9	7.0	9.3
D23	27.8	6.6	10.4
D24	23.6	6.3	14.5
D25	26.6	6.5	12.7

Among the experimental groups that were evaluated, the D13 configuration (4% SAE, 0.1% FA, and 5% SF) exhibited the most robust performance synergy, characterised by a compressive strength of 35.2 MPa, a flexural strength of 7.5 MPa, and a minimised water absorption of 8.0%. This optimal response is attributed to a multi-scale coupling effect: the coalesced polymer membranes enhance matrix-aggregate adhesion, the trace-level air

entrainment refines the pore topology without inducing structural instability, and the straw fibres provide a dense 3D bridging network to arrest crack propagation. Consequently, the D13 mixing proportion is regarded as the standard formulation for engineering high-performance VSLAC with optimised mechanical and permeation resistance.

3.4.2. Comparative Experimental Analysis

The present study employed a comparative methodology to evaluate the long-term durability of the engineering composite materials. In this regard, the optimised VSLAC was compared and tested with the control group. This multidimensional durability assessment encompassed apparent density, water absorption, permeability, thermal conductivity, and frost resistance (Figure 12A). The experimental dataset reveals a systematic enhancement across all investigated parameters, thus validating the efficacy of the multi-scale modification strategy. A marginal increase in apparent density was recorded, which is a direct manifestation of the multi-scale pore-occlusion effect induced by the supplementary admixtures. This serves as a critical indicator of structural densification [46].

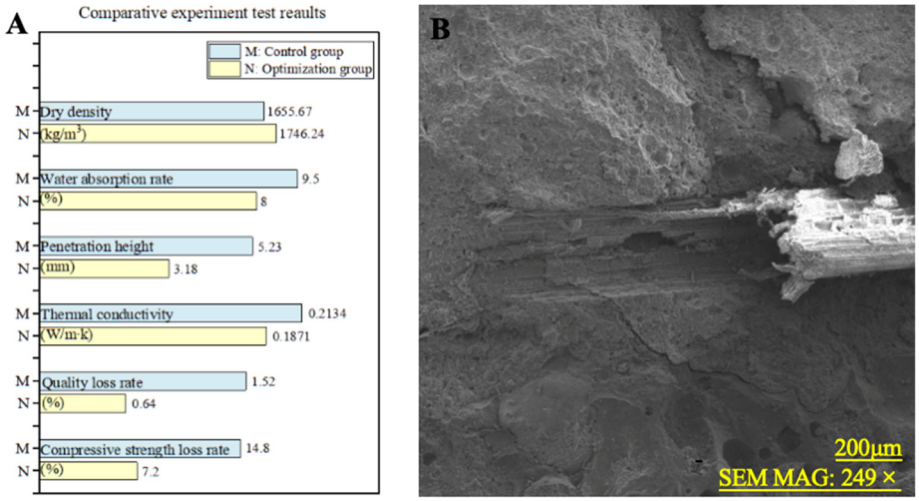


Figure 12. (**A**) Comparative experiment teat results. (**B**) Microstructure of scoria concrete prepared with optimal mix ratio.

The synergy between SAE and FA proved instrumental in the refinement of the internal micro-architecture. It has been demonstrated that the optimisation of the pore-filling efficiency has the effect of curtailing capillary suction and bolstering resistance to chloride ion penetration. In this manner, the penetration depth is restricted to a mere 3.18 mm. Such microstructural refinement provides the fundamental basis for the material's resilience against more severe environmental stressors, particularly cyclic temperature fluctuations.

With regard to the durability of frost, the incorporation of SF was identified as the pivotal factor in mitigating damage caused by low temperatures. Following exposure to 50 freeze–thaw cycles, the modified VSLAC demonstrated notable structural resilience, exhibiting a compressive strength loss of 7.2%, representing a 50% improvement over the baseline. Additionally, mass loss was minimised to an insignificant 0.64%. This enhanced endurance is fundamentally rooted in the 3D spatial network established by the fibres. The SF network has been shown to effectively bridge micro-cracks and redistribute internal stresses generated by hydraulic and cryostatic pressures. This inhibition of crack coalescence and retardation of structural degradation ensures the mechanical integrity of the matrix under cyclic cryogenic loading [53,55].

The synergistic interaction among SF, FA, and SAE reinforces the internal connectivity of the cementitious matrix, yielding a refined pore architecture and a densified ITZ. This mi-

crostructural optimisation is instrumental in suppressing thermal flux, thereby enhancing the insulating efficacy of the composite [17]. A numerical analysis was conducted utilising the abaqus software (Abaqus 2022) programme in order to evaluate the constitutive behaviour of concrete under compression. The resulting stress–strain profiles (Figure 13) exhibit divergent mechanical trajectories between the two cohorts: the baseline VSLAC yielded a peak stress of 19.47 MPa at a strain of 0.0029, whereas the optimized VSLAC manifested a superior mechanical response, with the peak stress ascending to 29.5 MPa (a 51.5% enhancement) and the corresponding strain reaching 0.0076 (a 162% increase) [50].

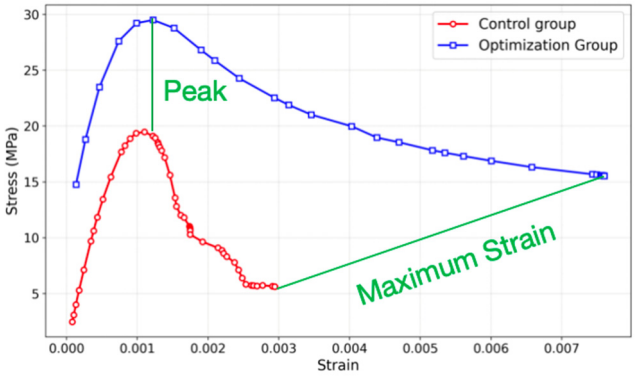


Figure 13. Stress–strain curve comparison.

A comprehensive examination of mono- and multi-incorporation regimes has been undertaken to elucidate the mechanisms underpinning the multi-scale optimisation of VSLAC. ITZ cohesion and interfacial integrity are substantially bolstered at a 4% SAE concentration, with polymer particles effectively occluding scoria and matrix pores, thereby maximising load-bearing capacity. In the context of the FA series, it has been demonstrated that a 0.1% dosage is optimally efficacious in terms of rheological properties and packing density. While higher FA concentrations have been shown to decrease thermal conductivity, the 0.1% threshold is critical to prevent structural instability and maintain durability. With regard to the utilisation of SF reinforcement, longitudinal data has been demonstrated to substantiate that alkali-pretreated fibres exhibit a marked improvement in performance when compared with their untreated counterparts. Although peak compressive and flexural strengths were recorded at 3% and 5% SF, respectively, the 5% dosage was identified as the optimal concentration to synergistically balance seismic energy dissipation with thermal insulation.

It is noteworthy that the optimal dosages derived from individual admixture trials align with the results of the D13 group from the orthogonal test matrix. This mutual validation process serves to confirm the reliability of the proposed formulation. Consequently, the optimal admixture regime for high-performance VSLAC is established as 4% SAE, 0.1% FA, and 5% SF.

3.5. Fabrication Morphology and Failure Modes

As demonstrated in Figure 14A, the VSLAC specimens prepared without chemical admixtures exhibited pronounced aggregate flotation and phase stratification, characterised by the upward migration of the lightweight scoria. In contrast, the incorporation of SAE mitigated these segregation tendencies by leveraging the polymer's viscosity-enhancing properties, which bolstered the cohesive forces between the aggregates and the cementitious paste. This synergistic interaction yielded a homogeneous distribution and a refined surface finish post-vibration. Upon reaching the 28-day curing milestone (Figure 14C), the modified specimens exhibited structural uniformity with no discernible evidence of the flotation or

layering observed in the control group, thus confirming the efficacy of SAE in ensuring matrix-aggregate stability.



Figure 14. States of VSALC: (**A**) as-prepared mixture, (**B**) mixture after mold vibration and (**C**) optimized mixture state.

Shear failure is a predominant degradation mode in concrete structures. In this investigation, the primary function of SAE was to reinforce the cohesive integrity of the cementitious matrix, while SF was incorporated to enhance the flexural resilience of the composite. As illustrated in Figure 15A, the baseline mineral admixture specimens demonstrated a distinctive conical shear failure upon reaching the ultimate compressive load, indicative of inherent macroscopic brittleness. Conversely, the specimens fortified with SF exhibited the capacity to preserve structural integrity without undergoing catastrophic disintegration during the loading sequence (Figure 15B). This phenomenon underscores the efficacy of fibre reinforcement in significantly elevating the energy dissipation capacity, thereby facilitating a transition from a brittle fracture regime to a quasi-ductile failure mode. Consequently, the synergistic integration of SF and SAE substantially augments the fracture toughness and post-peak deformability of the VSLAC.

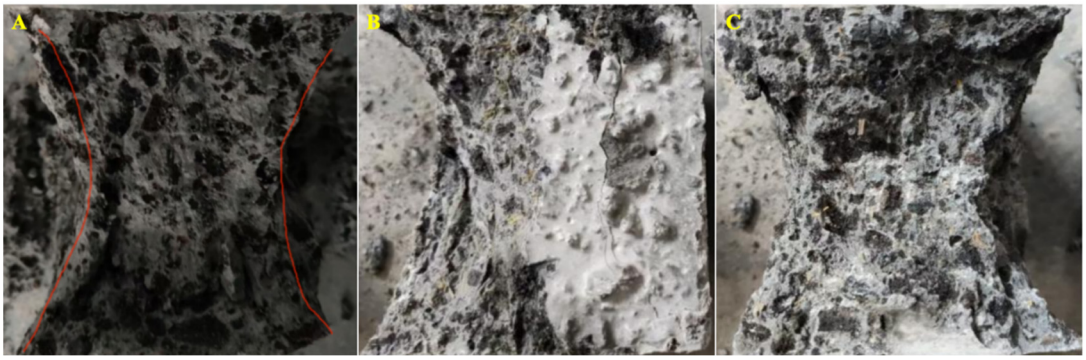


Figure 15. (**A**) Failure morphology of plain VSALC (The red line represents the failure pattern of the standard concrete specimens.). (**B**) Failure morphology of optimized VSALC. (**C**) Internal cross-section subsequent to the division of the failed specimen.

4. Conclusions

The present study executed a systematic multi-scale optimisation of VSLAC. The integration of macroscopic performance metrics with microstructural characterisation has enabled the establishment of the following conclusions:

a. Synergistic Efficacy of Binary SCMs: The binary incorporation of 10% fly ash and 10% GGBS resulted in a potent synergy between pozzolanic reaction kinetics and physical packing mechanisms. This combination effectively densified the cementitious matrix while reducing inter-particle friction, thereby optimising the rheological behaviour of the fresh paste. Consequently, the modified binder system yielded a 28-day

compressive strength of 28.8 MPa, representing a 20% enhancement relative to the control cohort.

b. The Mechanistic Influence of Discrete Admixtures: The present study has demonstrated that individual admixture analysis can reveal substantial improvements in interfacial adhesion, as evidenced by a 4% SAE, which has been shown to yield a 40% gain in flexural capacity. The FA at a 0.1% threshold has been demonstrated to refine pore topology and rheology; however, supra-optimal concentrations have been shown to trigger detrimental macropore coalescence and subsequent mechanical deterioration. Furthermore, the 5% alkali-treated SF establishes a robust 3D bridging scaffold, successfully transitioning the failure mechanism from a brittle fracture regime to a quasi-ductile response.

c. Ternary Synergistic Optimization: The orthogonal experimental design identifies the D13 configuration (4% SAE, 0.1‰ FA, and 5% SF) as the optimal formulation. The ternary system is found to yield superior mechanical and physical properties, including a compressive strength of 35.2 MPa, a flexural strength of 7.5 MPa, and a minimised water absorption of 8.0%. In comparison with the baseline, the optimised VSLAC exhibited a 51.4% reduction in strength degradation following freeze–thaw cycles and a 12.3% decrease in thermal conductivity, demonstrating exceptional environmental resilience.

d. Micro-evolution and structural stability: The micro-analytical validation process, encompassing both SEM and Abaqus, has been undertaken to ascertain the efficacy of the synergistic interaction among admixtures. The findings of this process have been corroborated and substantiated, thus confirming that the aforementioned admixtures indeed promote ITZ densification and pore architecture refinement. The sealing effect of SAE and FA on the vesicular scoria surface, coupled with the crack-arresting action of SF, effectively suppresses aggregate flotation and phase stratification. The process ensures macro-homogeneity and structural integrity of the VSLAC composite.

e. Prospective Outlook: Whilst the present study has demonstrated an enhancement in the immediate performance of the enhanced VSLAC, subsequent research should focus on aspects such as artificial intelligence (AI), automated long-term carbonation kinetics, creep behaviour, and the stability of alkali-aggregate reactions. Furthermore, a full life cycle assessment and technical economic analysis should be conducted to verify the environmental benefits and commercial feasibility of this material for large-scale application in sustainable ultra-low energy buildings [56–58].

Author Contributions: Conceptualization, J.Z.; methodology, J.Z. and R.L.; software, J.Z. and R.L.; validation, J.Z., R.L. and G.X.; resources, J.Z. and R.L.; data curation, J.Z.; writing—original draft preparation, J.Z. and R.L.; writing—review and editing, J.Z., R.L. and G.X.; funding, J.Z. and G.X. All authors have read and agreed to the published version of the manuscript.

Funding: This research was supported by the Beijing Technology and Business University's lateral project funding (Project No.: 20250066) and the National Key Research and Development Program of China (Project No.: 2018YFD1101000).

Data Availability Statement: The original contributions presented in this study are included in the article. Additional questions can be directed to the corresponding author.

Conflicts of Interest: Author Jinhong Zhang was employed by Jiangsu Qiqing New Material Technology Co., Ltd. The remaining authors declare that the research was conducted in the absence of any commercial or financial relationships that could be construed as a potential conflict of interest.

Abbreviations

The following abbreviations are used in this manuscript:

VS	Volcanic Scoria
VSLAC	Volcanic Scoria Lightweight Aggregate Concrete
OPC	Ordinary Portland Cement
GGBS	Ground Granulated Blast Furnace Slag
SAE	Styrene-acrylic Emulsion
FA	Foaming Agent
SF	Straw Fibre
ITZ	Interfacial Transition Zone
SEM	Scanning Electron Microscopy
SCMs	Supplementary Cementitious Materials
LWAC	Lightweight Aggregate Concrete
PCE	Polycarboxylate-based

References

1. Onoue, K.; Tamai, H.; Suseno, H. Shock-Absorbing Capability of Lightweight Concrete Utilizing Volcanic Pumice Aggregate. *Constr. Build. Mater.* **2015**, *83*, 261–274. [CrossRef]
2. Sahoo, C.; Sahoo, S.K.; Das, M.; Mishra, S.P. Lightweight Aggregate Concrete: Strength Analysis. *Curr. J. Appl. Sci. Technol.* **2022**, *41*, 32–41. [CrossRef]
3. Mo, K.H.; Ling, T.-C.; Alengaram, U.J.; Yap, S.P.; Yuen, C.W. Overview of Supplementary Cementitious Materials Usage in Lightweight Aggregate Concrete. *Constr. Build. Mater.* **2017**, *139*, 403–418. [CrossRef]
4. Cavalline, T.L.; Gallegos, J.; Castrodale, R.W.; Freeman, C.; Liner, J.; Wall, J. Influence of Lightweight Aggregate Concrete Materials on Building Energy Performance. *Buildings* **2021**, *11*, 94. [CrossRef]
5. Abed, M.A.; Anagreh, A.; Tošić, N.; Alkhabbaz, O.; Alshwaiki, M.E.; Černý, R. Structural Performance of Lightweight Aggregate Concrete Reinforced by Glass or Basalt Fiber Reinforced Polymer Bars. *Polymers* **2022**, *14*, 2142. [CrossRef] [PubMed]
6. Zhou, D.; Yang, X.; Miao, Y.; Chen, T.; Yao, Z. A Study of Energy Dissipation of Polypropylene Fiber Reinforced Recycled Concrete Under Uniaxial Compression. *Mech. Compos. Mater.* **2024**, *60*, 717–728. [CrossRef]
7. Rathika, M.; Ravichandran, P.T.; Ramasubramani, R. Experimental Investigation on the Mechanical Properties and Microstructure Behaviour of Concrete Using Lightweight Expanded Clay Aggregate (LECA) with Admixture. In *AIP Conference Proceedings*; AIP Publishing: Melville, NY, USA, 2024; Volume 3187, p. 030004.
8. Agrawal, Y.; Gupta, T.; Sharma, R.; Panwar, N.L.; Siddique, S. A Comprehensive Review on the Performance of Structural Lightweight Aggregate Concrete for Sustainable Construction. *Constr. Mater.* **2021**, *1*, 39–62. [CrossRef]
9. Hong, W.; Shen, C.; Zhu, X. Assessing the Potential of Recycled Fine Aggregate from Freeze-Thawed Parent Concrete for Structural Concrete. *Mater. Res. Express* **2023**, *10*, 125504. [CrossRef]
10. Sua-iam, G.; Makul, N. Recycling Prestressed Concrete Pile Waste to Produce Green Self-Compacting Concrete. *J. Mater. Res. Technol.* **2023**, *24*, 4587–4600. [CrossRef]
11. Alyaseen, A.; Poddar, A.; Kumar, N.; Sihag, P.; Lee, D.; Kumar, R.; Singh, T. Assessing the Compressive and Splitting Tensile Strength of Self-Compacting Recycled Coarse Aggregate Concrete Using Machine Learning and Statistical Techniques. *Mater. Today Commun.* **2024**, *38*, 107970. [CrossRef]
12. Wang, Y.; Li, J.; Miao, W.; Su, Y.; He, X.; Strnadel, B. Preparation and Characterizations of Hydroxyapatite Microcapsule Phase Change Materials for Potential Building Materials. *Constr. Build. Mater.* **2021**, *297*, 123576. [CrossRef]
13. Shah, S.J.; Naeem, A.; Hejazi, F.; Mahar, W.A.; Haseeb, A. Experimental Investigation of Mechanical Properties of Concrete Mix with Lightweight Expanded Polystyrene and Steel Fibers. *CivilEng* **2024**, *5*, 209–223. [CrossRef]
14. Alharthai, M.; Ali, T.; Qureshi, M.Z.; Ahmed, H. The Enhancement of Engineering Characteristics in Recycled Aggregates Concrete Combined Effect of Fly Ash, Silica Fume and PP Fiber. *Alex. Eng. J.* **2024**, *95*, 363–375. [CrossRef]
15. Geetha, S.; Sree Varrun, D.; Sathya Sudhan, S.; Muthuraja, V. Studies on Properties of Polymer Modified Aerated Concrete. *Mater. Today Proc.* **2023**, *80*, 870–876. [CrossRef]
16. He, Q. A Unified Metric Architecture for AI Infrastructure: A Cross-Layer Taxonomy Integrating Performance, Efficiency, and Cost. *arXiv* **2025**, arXiv:2511.21772.
17. Shi, C.; Li, M.; Ma, C.; He, T. Interfacial Bonding Properties of Styrene-Butadiene Rubber and Ethylene Vinyl Acetate Emulsion-Modified OPC–CAC–G Repair Mortar. *Constr. Build. Mater.* **2023**, *370*, 130747. [CrossRef]
18. He, Q.; Qu, C. Waste-to-Energy-Coupled AI Data Centers: Cooling Efficiency and Grid Resilience. *arXiv* **2025**, arXiv:2512.24683.

19. Sun, D.; Fan, X.; Zhang, B.; Ding, F.; Wu, R.; Zhang, Z. Early-Age Autogenous Shrinkage Control in Nano-$CaCO_3$ Modified Concrete Using Superabsorbent Polymer Internal Curing. *J. Build. Eng.* **2025**, *116*, 114731. [CrossRef]
20. Liu, Y.; Liu, Z.; Rong, H.; Ma, G. Research on the Foaming Mechanism of Microbial Foaming Agent and Its Application in Foam Concrete. *Constr. Build. Mater.* **2023**, *379*, 131041. [CrossRef]
21. Bian, P.; Zhang, M.; Yu, Q.; Zhan, B.; Gao, P.; Guo, B.; Chen, Y. Prediction Model of Compressive Strength of Foamed Concrete Considering Pore Size Distribution. *Constr. Build. Mater.* **2023**, *409*, 133705. [CrossRef]
22. Gołaszewska, M.; Gołaszewski, J.; Klemczak, B.; Koenders, E.A.B. Effect of Foaming Agent and Admixtures on Hydration in Ultralight Foam Concrete with Cement-Metakaolin Binders. *J. Build. Eng.* **2025**, *104*, 112365. [CrossRef]
23. Deshpande, A.A.; Kumar, D.; Ranade, R. Temperature Effects on the Bond Behavior between Deformed Steel Reinforcing Bars and Hybrid Fiber-Reinforced Strain-Hardening Cementitious Composite. *Constr. Build. Mater.* **2020**, *233*, 117337. [CrossRef]
24. Wang, X.; Wu, Q.; Chen, W. Experimental Study on the Impact Resistance of Steel Fiber Reinforced All-Lightweight Concrete Beams under Single and Hybrid Mixing Conditions. *Buildings* **2023**, *13*, 1251. [CrossRef]
25. Yan, Y.; Xing, Z.; Chen, X.; Xie, Z.; Zhang, J.; Chen, Y. Axial Compression Performance of CFST Columns Reinforced by Ultra-High-Performance Nano-Concrete under Long-Term Loading. *Nanotechnol. Rev.* **2023**, *12*, 20220537. [CrossRef]
26. Amin, M.N.; Khan, K.; Abu Arab, A.M.; Farooq, F.; Eldin, S.M.; Javed, M.F. Prediction of Sustainable Concrete Utilizing Rice Husk Ash (RHA) as Supplementary Cementitious Material (SCM): Optimization and Hyper-Tuning. *J. Mater. Res. Technol.* **2023**, *25*, 1495–1536. [CrossRef]
27. Wu, Z.; Wang, X.; Chen, Z. Experimental Study on Preparation and Performance of the Corn Straw Fiber (CSF) Reinforced EPS Concrete. *J. Build. Eng.* **2024**, *89*, 109378. [CrossRef]
28. Fan, D.; Zhu, X.; Xiang, Z.; Lu, Y.; Quan, L. Dimension-Reduction Many-Objective Optimization Design of Multimode Double-Stator Permanent Magnet Motor. *IEEE Trans. Transp. Electrific.* **2025**, *11*, 1984–1994. [CrossRef]
29. Liu, J.; Zhao, W.; Li, L. Effects of Nano-SiO_2 Grafting on Improving the Interfacial and Mechanical Properties of Concrete with Rice Straw Fibers. *Constr. Build. Mater.* **2023**, *398*, 132516. [CrossRef]
30. Wu, X.; Wang, H.; Zhang, Y.; Zou, B.; Hong, H. A Tutorial-Generating Method for Autonomous Online Learning. *IEEE Trans. Learn. Technol.* **2024**, *17*, 1532–1541. [CrossRef]
31. Althoey, F.; Zaid, O.; Martínez-García, R.; de Prado-Gil, J.; Ahmed, M.; Yosri, A.M. Ultra-High-Performance Fiber-Reinforced Sustainable Concrete Modified with Silica Fume and Wheat Straw Ash. *J. Mater. Res. Technol.* **2023**, *24*, 6118–6139. [CrossRef]
32. Hong, S.-H.; Choi, J.-S.; Lee, J.; Yoon, Y.-S. Optimal Mix Design and Quality Properties of 50 MPa Self-Consolidating Lightweight Concrete. *J. Korean Soc. Hazard Mitig.* **2020**, *20*, 135–142. [CrossRef]
33. Lin, J.; Wang, Y.; Li, M.; Chen, H.; Cao, H.; Jing, C. Continuum Percolation of the Realistic Nonuniform ITZs in 3D Polyphase Concrete Systems Involving the Aggregate Shape and Size Differentiation. *Sci. Eng. Compos. Mater.* **2024**, *31*, 20220237. [CrossRef]
34. Ahmed, A.R.; Yamany, M.E.; Kholy, A.E. High Strength Lightweight Concrete, Using Scoria and Mineral Admixture. *Int. J. Membr. Sci. Technol.* **2023**, *10*, 3463–3471. [CrossRef]
35. Liu, J.; Xie, X.; Li, L. Experimental Study on Mechanical Properties and Durability of Grafted Nano-SiO_2 Modified Rice Straw Fiber Reinforced Concrete. *Constr. Build. Mater.* **2022**, *347*, 128575. [CrossRef]
36. Wang, T.; Gao, X.; Li, Y.; Liu, Y. An Orthogonal Experimental Study on the Influence of Steam-Curing on Mechanical Properties of Foam Concrete with Fly Ash. *Case Stud. Constr. Mater.* **2024**, *20*, e02665. [CrossRef]
37. Abbas, S.N.; Qureshi, M.I. An Investigation of Mechanical Properties of Self Compacting Concrete (SCC) after Addition of Ground Granulated Blast Furnace Slag (GGBFS) and Fly Ash (FA). *Mater. Chem. Phys. Sustain. Energy* **2025**, *2*, 100008. [CrossRef]
38. Yan, G.; Hu, J.; Chen, M.; Ma, Y.; Huang, H.; Zhang, Z.; Wei, J.; Shi, C.; Yu, Q. Performance Evaluation of Reinforced Slag-Fly Ash-Ceramic Waste Powders Ternary Geopolymer Concrete under Chloride Ingress Environment. *Constr. Build. Mater.* **2025**, *478*, 141447. [CrossRef]
39. Araújo, L.B.R.; de Souza, M.L.; Melo, A.R.S.; Costa, H.N.; Babadopulos, L.F.A.L.; Cabral, A.E.B.; Pileggi, R.G. High-Strength Self-Compacting Alkali-Activated Concrete Produced with Fly Ash and Steel Slag: Rheological Behavior and Mixing Rheology Comparisons with a Portland Cement Concrete. *CEMENT* **2025**, *22*, 100156. [CrossRef]
40. Tay, C.H.; Mazlan, N.; Wayayok, A.; Basri, M.S.; Albakri Abdullah, M.M. Zeolite Based Foamed Geopolymer Concrete Reinforced with Cellulose Nanofibril Prepared in Low Concentration Alkaline Solution: Porosity, Compressive Strength, and Water Permeability. *J. Clean. Prod.* **2025**, *489*, 144609. [CrossRef]
41. Zhang, J.; Fu, W. Sponge Effect of Aerated Concrete on Phosphorus Adsorption-Desorption from Agricultural Drainage Water in Rainfall. *Soil Water Res.* **2020**, *15*, 220–227. [CrossRef]
42. Zhang, Y.; Gu, K.; Liu, J.; Zheng, X.; Qiu, W.; Wang, Y.; Tan, H. Effect of C-S-H/PCE on Compressive Strength and Carbonation Resistance of Foamed Concrete. *Constr. Build. Mater.* **2025**, *495*, 143548. [CrossRef]
43. Falliano, D.; Parmigiani, S.; Suarez-Riera, D.; Ferro, G.A.; Restuccia, L. Stability, Flexural Behavior and Compressive Strength of Ultra-Lightweight Fiber-Reinforced Foamed Concrete with Dry Density Lower than 100 Kg/M3. *J. Build. Eng.* **2022**, *51*, 104329. [CrossRef]

44. Vinod, B.R.; Surendra, H.J.; Shobha, R. Lightweight Concrete Blocks Produced Using Expanded Polystyrene and Foaming Agent. *Mater. Today Proc.* **2022**, *52*, 1666–1670. [CrossRef]
45. Majeed, S.S.; Othuman Mydin, M.A.; Bahrami, A.; Dulaimi, A.; Özkılıç, Y.O.; Omar, R.; Jagadesh, P. Development of Ultra-Lightweight Foamed Concrete Modified with Silicon Dioxide (SiO_2) Nanoparticles: Appraisal of Transport, Mechanical, Thermal, and Microstructural Properties. *J. Mater. Res. Technol.* **2024**, *30*, 3308–3327. [CrossRef]
46. Mostafa, S.A.; Agwa, I.S.; Elboshy, B.; Zeyad, A.M.; Seddik Hassan, A.M. The Effect of Lightweight Geopolymer Concrete Containing Air Agent on Building Envelope Performance and Internal Thermal Comfort. *Case Stud. Constr. Mater.* **2024**, *20*, e03365. [CrossRef]
47. Luo, Z.; Zhang, X.; Liu, X.; Tian, C.; Liu, L.; Chen, Z.; Tan, H.; Yang, H. Effects of Styrene-Acrylic Emulsion on Toughness, Volume Stability and Fiber Dispersion of Hybrid Fibers Reinforced Ultra-High Performance Geopolymer Concrete. *Constr. Build. Mater.* **2025**, *473*, 140930. [CrossRef]
48. Jiao, H.; Chen, X.; Yang, Y.; Chen, X.; Yang, L.; Yang, T. Mechanical Properties and Meso-Structure of Concrete under the Interaction between Basalt Fiber and Polymer. *Constr. Build. Mater.* **2023**, *404*, 133223. [CrossRef]
49. Moelich, G.M.; Kruger, P.J.; Combrinck, R. Mitigating Early Age Cracking in 3D Printed Concrete Using Fibres, Superabsorbent Polymers, Shrinkage Reducing Admixtures, B-CSA Cement and Curing Measures. *Cem. Concr. Res.* **2022**, *159*, 106862. [CrossRef]
50. Fan, Z.; Liu, H.; Liu, G.; Wang, X.; Cui, W. Compressive Performance of Fiber Reinforced Recycled Aggregate Concrete by Basalt Fiber Reinforced Polymer-Polyvinyl Chloride Composite Jackets. *J. Renew. Mater.* **2023**, *11*, 1763–1791. [CrossRef]
51. Zhang, S.; Qi, X.; Guo, S.; Zhang, L.; Ren, J. A Systematic Research on Foamed Concrete: The Effects of Foam Content, Fly Ash, Slag, Silica Fume and Water-to-Binder Ratio. *Constr. Build. Mater.* **2022**, *339*, 127683. [CrossRef]
52. Huang, J.; Qiu, S.; Rodrigue, D. Parameters Estimation and Fatigue Life Prediction of Sisal Fibre Reinforced Foam Concrete. *J. Mater. Res. Technol.* **2022**, *20*, 381–396. [CrossRef]
53. Lura, P.; Toropovs, N.; Justs, J.; Shakoorioskooie, M.; Münch, B.; Griffa, M. Mitigation of Plastic Shrinkage Cracking with Natural Fibers—Kenaf, Abaca, Coir, Jute and Sisal. *Cem. Concr. Compos.* **2024**, *155*, 105827. [CrossRef]
54. Hasan, N.S.; Shaurdho, N.M.N.; Basit, A.; Paul, S.C.; Sobuz, H.R.; Miah, M.J. Assessment of the Rheological and Mechanical Properties of Palmyra Fruit Mesocarp Fibre Reinforced Eco-Friendly Concrete. *Constr. Build. Mater.* **2023**, *407*, 133530. [CrossRef]
55. Yang, W.; Huang, Y.; Li, C.; Tang, Z.; Quan, W.; Xiong, X.; He, J.; Wu, W. Damage Prediction and Long-Term Cost Performance Analysis of Glass Fiber Recycled Concrete under Freeze-Thaw Cycles. *Case Stud. Constr. Mater.* **2024**, *21*, e03795. [CrossRef]
56. He, Q.; Qu, C. Modular Landfill Remediation for AI Grid Resilience. *arXiv* **2025**, arXiv:2512.19202. [CrossRef]
57. Liang, N.; Hu, X.; Zhang, X.; Li, W.; Guo, Z.; Huang, X.; Li, Z.; Zhang, R.; Shen, T.; Zou, X.; et al. Ratiometric Sensing for Ultratrace Tetracycline Using Electrochemically Active Metal–Organic Frameworks as Response Signals. *J. Agric. Food Chem.* **2023**, *71*, 7584–7592. [CrossRef] [PubMed]
58. Zhang, L.T.; Duan, Y.J.; Wang, Y.J.; Pineda, E.; Yang, Y.; Pelletier, J.M.; Kato, H.; Crespo, D.; Qiao, J.C. Creep and recovery behavior of metallic glasses in a global strain approach within transition state theory. *Acta Mech. Sin.* **2026**, *42*, 425311.

Disclaimer/Publisher's Note: The statements, opinions and data contained in all publications are solely those of the individual author(s) and contributor(s) and not of MDPI and/or the editor(s). MDPI and/or the editor(s) disclaim responsibility for any injury to people or property resulting from any ideas, methods, instructions or products referred to in the content.